

**FISCHER-TROPSCH DIESEL FROM
LOW RIBBLET RATIO SYNGAS
CATALYZED BY *nano*Fe-Co DISPERSED
HIERARCHICAL MFI ZEOLITE**

SHASHANK BAHRI



**DEPARTMENT OF CHEMICAL ENGINEERING
INDIAN INSTITUTE OF TECHNOLOGY DELHI,**

NOVEMBER 2021

©Indian Institute of Technology New Delhi-2021

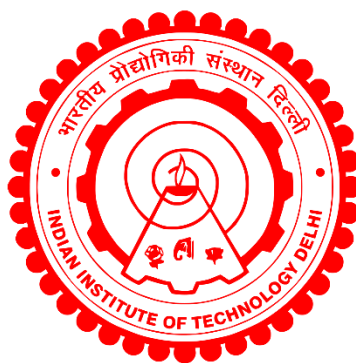
**FISCHER-TROPSCH DIESEL FROM
LOW RIBBLET RATIO SYNGAS
CATALYZED BY *nano*Fe-Co DISPERSED
HIERARCHICAL MFI ZEOLITE**

by

SHASHANK BAHRI
Department of Chemical Engineering

Submitted

in fulfilment of the requirements of the degree of Doctor of Philosophy
to the



INDIAN INSTITUTE OF TECHNOLOGY DELHI
NOVEMBER 2021

*Dedicated to all my Gurus and beloved family.
For their endless love, support and encouragement.*

CERTIFICATE

This is to certify that the thesis entitled, “**Fischer-Tropsch Diesel from Low Ribblet Ratio Syngas Catalyzed by *nano*Fe-Co Dispersed Hierarchical MFI Zeolite**” being submitted by Mr Shashank Bahri to the Indian Institute of Technology Delhi for the award of Doctor of Philosophy in Chemical Engineering is a record of bonafide research work carried out by him under my guidance and supervision. He has fulfilled the requirements for submitting the thesis, which has reached the required standard to the best of my knowledge.

The research report and results presented in this thesis have not been submitted, in part or full, to any other university or institute for awarding any degree or diploma.

(Dr. Sreedevi Upadhyayula)
CLASS of 66 Chair Professor
Department of Chemical Engineering
Indian Institute of Technology Delhi
Hauz Khas, New Delhi-110016

Acknowledgements

Many people helped me in completing my research and my thesis, some who were directly involved and others who were indirectly there to support me in rain and shine. It is my duty and my utmost pleasure to take a moment to thank them all for all that they have done for me and to acknowledge their continuous support in any way possible for them.

First and foremost, I would like to express my sincere gratitude towards my research advisor, **Prof. Sreedevi Upadhyayula**, for her constant guidance, motivation and inspiration throughout my research work. I have no words to thank her for her continuous support toward the timely evaluation of all my results, reports and journal papers. She created an environment filled with fun and excitement, and no frustration or burden was ever felt during my research. I acknowledge her for inculcating her technical skills and her systematic and positive approach towards research with deep gratitude. I can never imagine having a better advisor and mentor for my research. The laboratory experimentation could not have been this effortless without her unconditional support and friendly behavior. I am fortunate and blessed to have a guide like her.

Apart from my supervisor, I am grateful to the current Head of the Department, **Prof. A.K. Saroha** and Former Head, **Prof. Kamal Kishore Pant**, for their administrative support and constant encouragement to complete my thesis. I thank my research committee members **Prof. Kamal K. Pant, Prof. Vivek V. Buwa and Prof. K.A. Subramanian**, for their keen comments, encouragement, and particular suggestions, which inspired me to widen my research from various perspectives. I am incredibly thankful to **Prof. Veena Chaudhary, Prof. Rajni Jain, Prof. Rajesh Khanna and Prof. Sudharshan Ghosh** for their constant support, encouragement and valuable suggestions. In particular, I acknowledge the opportunity to work with **Prof. Anna M. Venezia**, ISMN-CNR, Italy and **Prof. Jalama Kalala**, University of Johannesburg, whose instruction and advice was indispensable at the start of my project work. I am thankful to **Dr. Pranab Rakshit** and **Dr. Rajiv Kumar** from Bharat Petroleum Corporate R&D Centre, Greater Noida, for helping in analytical equipment support.

I am thankful to all my seniors **Dr. Kishore Kondamudi, Mr. B. Pradeep Kumar**, and colleagues **Dr. Kaisar Ahmad, Dr. Komal Kumar, Dr. Gul Afreen, Mr. Uttaran Basak and Mr. Shailesh Pathak**, for their constant support and help to my research work. I appreciate my laboratory staff **Mr. Ashish Nayak** and **Mr. A.K. Gautam**, for

their help with my experimental sets/set-up and lab equipment. I am grateful to **Mr. Rajesh Kumar, Mr. Animesh Bhowal** and **Ms. Aastha Sharma**, Project Scientists in the Central Research Facility, for timely analysis of my samples.

I am blessed to have friends like **Dr. Firdaus Parveen, Dr. Rekha Yadav, Mr. Sagar Saxena** and **Ms. Neeta Prajapati**. We have shared both good and bad times, and they have always been there for me in times of need. The friendships that we have developed will last a lifetime. I am very grateful to my school teachers **Ms. Amarjeet Malhotra, Ms. Archana Tiwari** and **Ms. Nimisha Srivastava**, for laying the foundation of my successful educational journey.

I am fortunate to have **Mr. Narinder Nath Bahri** and **Ms. Kanta Rani** as my parents, and my aunty **Ms. Kamlesh** who supported me morally, financially, and in every aspect of my life. All this could not have been possible without their endless love, support and encouragement. I am very thankful to my sister for always being there for me in my good and bad times. My little angel, my niece **Vaidehi**, will always remain a source of encouragement, passion and motivation for me. Since her arrival, she has filled my life with immense joy and love. His smile alone takes all the fears and worries away from me. I thank my sisters **Ms. Radhika** and **Ms. Kamini** for their support throughout my research journey. I also acknowledge the loving memories of my grandmother **Ms. Chandrawati**.

Lastly, I thank almighty for his blessings and for surrounding me with such genuinely extraordinary people. I hereby express my hearty & sincere thanks to all those who have supported me, either directly or indirectly, in the successful completion of my research work successfully.

(Shashank Bahri)

ABSTRACT

The excessive utilisation of fossil fuel for meeting global energy demand leads to dwindling crude reserves, which develops an urge for alternative fuel production to meet global energy demands. Fischer-Tropsch synthesis is a commercially available technology capable of producing a broad range of gaseous, liquid and solid phase hydrocarbons using syngas with an approximate H_2/CO ratio in the range of 1.6-2. Fischer-Tropsch fuel has gained interest due to its better Internal-Combustion engine performance and NO_x and SO_x free emissions. The syngas used as a feedstock is generated from steam reforming of natural gas and gasification of coal, biomass, heavy petroleum residue and other carbonaceous waste. After removing contaminants, the cleaned syngas obtained has a low Ribblet ratio ($H_2 / (2CO+3CO_2) < 1$). In order to balance the Ribblet ratio, the additional energy-intensive pretreatment units involving H_2 enrichment and CO_2 absorption are installed before the Fischer-Tropsch reactors. Currently, direct utilisation of syngas with low Ribblet as a feedstock has become an aspect of consideration. High carbon utilisation in the Fischer-Tropsch process will improve energy efficiency, reduce production costs, and enhance industrial sustainability. The enormous amount of CO_2 released during syngas generation and from the Fischer-Tropsch tail-gas is added back to the FT reactor.

The present study focuses on the catalytic conversion of low Ribblet ratio syngas over Fe-Co bimetallic catalysts supported on *hierar*HZSM-5. Hierarchical pore structure was developed on HZSM-5 with silica to alumina mole ratio 50 using the post-synthetic modification technique. The catalytic activity of synthesized catalysts was tested in a laboratory-scale fixed-bed reactor. Fe-Co bimetallic active metals were loaded on *hierar*HZSM-5 varying Fe-Co ratio with a constant total metal loading of 30% using the sonication process to increase active metal dispersion. The advantage of incorporating Fe metal into Co catalyst was evidenced through positive CO_2 conversion and higher selectivity to diesel range hydrocarbons. Mechanistic studies reveal that the inter-conversion of the oxide and the carbide phases of active metals during the Fischer-Tropsch reaction conditions is responsible for carbon dioxide formation. Synergistic effect of milder Bronsted acidity and hierarchical porous structure of Fe-Co bimetallic catalyst supported over hierarchical HZSM-5 resulted in enhanced syngas conversion towards high-quality C_{11} - C_{20} range liquid synthetic fuel with stable catalytic activity for a longer time.

A series of 26 experiments were conducted using optimised Fe-2Co/*hierar*ZSM-5 catalyst for understanding the influence of a particular parameter and the synergy arising due to the second-order interaction among these process parameters. The experimental results were fitted into an empirical regression model, and the second-order Taylor series with a coefficient of determination (R^2) closer to 0.99 was used to approximate the process response. The developed regression models were statistically and experimentally validated. C₂-C₃ olefins play an essential role in deciding the chain growth. Thus, the relationship between C₂ and C₃ hydrocarbons was experimentally investigated over various process parameters.

In this study, the catalytic activity and stability of auxiliary iron introduced in different proximities to Co₃O₄ spinel are compared under the identical Fischer-Tropsch conditions for a continuous 120 hours' time-on-stream run. The spatial distance between different functionalities was monitored by various bulk and surface characterisations. A reconstructed partially inverse FeCo₂O₄ spinel with a closer and uniform iron and cobalt proximity shows superior catalytic performance with excellent stability ascribing to the interplay of cations having divalent and trivalent oxidation states in different geometric coordination. The cation substitution is found to tailor catalyst properties through modification in the preferential CO adsorption sites. The quantity and the nature of carbon deposited on the spent catalyst during optimal process conditions were also evaluated.

Further, the reaction mechanism and kinetics is investigated over the most promising catalyst. The combined transient IR and steady-state LHHW intrinsic kinetic model suggests the formation of HCO/HCOO⁻ intermediate species over Fe-Co sites. In order to derive a more reliable rate expression, simultaneous kinetics of Fischer-Tropsch and Water-Gas-Shift reactions are studied. The developed comprehensive reaction model postulates that the CO molecule adsorbed on FT active sites dissociates via a hydrogen assisted route and forms HCO intermediate species, and its subsequent reaction with atomic hydrogen (H^{*}) initiates chain growth. The hydrogenation of surface formyl (HCO) is the Fischer-Tropsch rate-controlling step more relevant than the other proposed elementary reactions. Finally, a three-layer Back Propagation Neural Network was tested and trained to predict the relation of non-linearity among the five process variables and the consumption rate of CO and total syngas. A similar prediction trend of CO and total syngas consumption rate provides evidence for the applicability of machine learning in modelling the kinetics of a complex gas-solid reaction.

सार

वैश्विक ऊर्जा मांग को पूरा करने के लिए जीवाश्म ईंधन के अत्यधिक उपयोग से कच्चे तेल के भंडार में कमी आती है, जिससे वैश्विक ऊर्जा मांगों को पूरा करने के लिए वैकल्पिक ईंधन उत्पादन की इच्छा पैदा होती है। फिशर-ट्रॉप्स संश्लेषण एक व्यावसायिक रूप से उपलब्ध तकनीक है जो 1.6-2 की सीमा में अनुमानित H₂/CO अनुपात के साथ सिनगैस का उपयोग करके गैसीय, तरल और ठोस चरण हाइड्रोकार्बन की एक विस्तृत श्रृंखला का उत्पादन करने में सक्षम है। फिशर-ट्रॉप्स ईंधन ने अपने बेहतर आईसी इंजन प्रदर्शन और एनओएक्स और एसओएक्स मुक्त उत्सर्जन के कारण रुचि प्राप्त की है। फीडस्टॉक के रूप में उपयोग किया जाने वाला सिनगैस प्राकृतिक गैस के भाप सुधार और कोयले, बायोमास, भारी पेट्रोलियम अवशेषों और अन्य कार्बनयुक्त कचरे के गैसीकरण से उत्पन्न होता है। दूषित पदार्थों को हटाने के बाद, प्राप्त साफ किए गए सिनगैस में कम रिबलेट अनुपात ($H_2/(2CO+3CO_2) < 1$) होता है। रिबलेट अनुपात को संतुलित करने के लिए, एफटी रिएक्टरों से पहले एच 2 संवर्धन और सीओ 2 अवशोषण से युक्त अतिरिक्त ऊर्जा-गहन प्रीट्रीटमेंट इकाइयां स्थापित की जाती हैं। वर्तमान में, फीडस्टॉक के रूप में कम रिबलेट वाले सिनगैस का प्रत्यक्ष उपयोग विचार का एक पहलू बन गया है। एफटी प्रक्रिया में उच्च कार्बन उपयोग से ऊर्जा दक्षता में सुधार होगा, उत्पादन लागत कम होगी और औद्योगिक स्थिरता में वृद्धि होगी। सिनगैस उत्पादन के दौरान और एफटी टेल-गैस से जारी CO₂ की भारी मात्रा को वापस एफटी रिएक्टर में जोड़ा जाता है।

वर्तमान अध्ययन *hierat*HZSM-5 पर समर्थित Fe-Co बाईमेटेलिक उत्प्रेरकों पर कम रिबलेट अनुपात सिनगैस के उत्प्रेरक रूपांतरण पर केंद्रित है। पोस्ट-सिंथेटिक संशोधन तकनीक का उपयोग करके सिलिका से एल्यूमिना मोल अनुपात 50 के साथ HZSM-5 पर पदानुक्रमित छिद्र संरचना विकसित की गई थी। संश्लेषित उत्प्रेरकों की उत्प्रेरक गतिविधि का परीक्षण प्रयोगशाला-स्तरीय फिक्स्ड-बेड रिएक्टर में किया गया था। Fe-Co बाईमेटेलिक सक्रिय धातुओं को *hierat*HZSM-5 भिन्न Fe-Co अनुपात पर लोड किया गया था, जिसमें सक्रिय धातु फैलाव को बढ़ाने के लिए sonication प्रक्रिया का उपयोग करके 30% की निरंतर कुल धातु लोडिंग होती है। सह उत्प्रेरक में Fe धातु को शामिल करने का लाभ सकारात्मक CO₂ रूपांतरण और डीजल श्रेणी के हाइड्रोकार्बन के लिए उच्च चयनात्मकता के माध्यम से प्रमाणित किया गया था। यांत्रिक अध्ययनों से पता चलता है कि फिशर-ट्रॉप्स प्रतिक्रिया स्थितियों के दौरान ऑक्साइड और सक्रिय धातुओं के कार्बाइड चरणों का अंतर-रूपांतरण कार्बन डाइऑक्साइड गठन के लिए जिम्मेदार है। माइल्ड ब्रॉस्टेड अम्लता का सहक्रियात्मक प्रभाव और पदानुक्रमित HZSM-5 पर समर्थित Fe-Co बाईमेटेलिक उत्प्रेरक की पदानुक्रमित झरझरा संरचना के परिणामस्वरूप लंबे समय तक स्थिर उत्प्रेरक गतिविधि के साथ उच्च गुणवत्ता वाले C₁₁-C₂₀ श्रेणी के तरल सिंथेटिक ईंधन के लिए सिनगैस रूपांतरण में वृद्धि हुई।

एक विशेष पैरामीटर के प्रभाव और इन प्रक्रिया मापदंडों के बीच दूसरे क्रम की बातचीत के कारण उत्पन्न होने वाले तालमेल को समझने के लिए अनुकूलित Fe-2Co/hieratHZSM-5 उत्प्रेरक का उपयोग करके 26 प्रयोगों की एक श्रृंखला आयोजित की गई थी। प्रायोगिक परिणामों को एक अनुभवजन्य प्रतिगमन मॉडल में फिट किया गया था, और दूसरे क्रम की टेलर श्रृंखला का निर्धारण गुणांक (R^2) के साथ 0.99 के करीब प्रक्रिया प्रतिक्रिया का अनुमान लगाने के लिए किया गया था। विकसित प्रतिगमन मॉडल सांख्यिकीय और प्रयोगात्मक रूप से मान्य थे। C₂-C₃ ओलेफिन श्रृंखला वृद्धि को तय करने में एक आवश्यक भूमिका निभाते हैं। इस प्रकार, विभिन्न प्रक्रिया मापदंडों पर C₂ और C₃ हाइड्रोकार्बन के बीच संबंधों की प्रयोगात्मक रूप से जांच की गई।

इस अध्ययन में, Co₃O₄ स्पिनल के लिए अलग-अलग निकटता में पेश किए गए सहायक लोहे की उत्प्रेरक गतिविधि और स्थिरता की तुलना समान फिशर-ट्रॉप्स स्थितियों के तहत लगातार 120 घंटे के टाइम-ऑन-स्ट्रीम रन के लिए की जाती है। विभिन्न कार्यात्मकताओं के बीच स्थानिक दूरी की निगरानी विभिन्न थोक और सतही विशेषताओं द्वारा की गई थी। एक करीब और एकसमान लोहे और कोबाल्ट निकटता के साथ आंशिक रूप से उलटा FeCo₂O₄ स्पिनल, विभिन्न ज्यामितीय समन्वय में द्विसंयोजक और त्रिसंयोजक ऑक्सीकरण राज्यों वाले उद्धरणों के परस्पर क्रिया के लिए उत्कृष्ट स्थिरता के साथ बेहतर उत्प्रेरक प्रदर्शन को दर्शाता है। तरजीही सीओ सोखना साइटों में संशोधन के माध्यम से उत्प्रेरक गुणों को दर्जी के लिए कटियन प्रतिस्थापन पाया जाता है। इष्टतम प्रक्रिया स्थितियों के दौरान खर्च किए गए उत्प्रेरक पर जमा कार्बन की मात्रा और प्रकृति का भी मूल्यांकन किया गया था।

इसके अलावा, सबसे आशाजनक उत्प्रेरक पर प्रतिक्रिया तंत्र और कैनेटीक्स की जांच की जाती है। संयुक्त क्षणिक IR और स्थिर-अवस्था LHHW आंतरिक गतिज मॉडल Fe-Co साइटों पर HCO/HCOO⁻ मध्यवर्ती प्रजातियों के गठन का सुझाव देता है। अधिक विश्वसनीय दर अभिव्यक्ति प्राप्त करने के लिए, फिशर-ट्रॉप्स और वाटर-गैस-शिफ्ट प्रतिक्रियाओं के एक साथ कैनेटीक्स का अध्ययन किया जाता है। विकसित व्यापक प्रतिक्रिया मॉडल यह मानता है कि एफटी सक्रिय साइटों पर adsorbed CO अणु एक हाइड्रोजन सहायता प्राप्त मार्ग के माध्यम से अलग हो जाता है और HCO मध्यवर्ती प्रजातियों का निर्माण करता है, और परमाणु हाइड्रोजन (H*) के साथ इसकी बाद की प्रतिक्रिया श्रृंखला वृद्धि की शुरुआत करती है। सतह फॉर्माइल (एचसीओ) का हाइड्रोजनीकरण अन्य प्रस्तावित प्राथमिक प्रतिक्रियाओं की तुलना में फिशर-ट्रॉप्स दर-नियंत्रित कदम अधिक प्रासंगिक है। अंत में, एक तीन-परत बैंक प्रोपेगेशन न्यूरल नेटवर्क का परीक्षण किया गया और पांच प्रक्रिया चर और सीओ की खपत दर और कुल सिनगैस के बीच गैर-रैखिकता के संबंध की भविष्यवाणी करने के लिए प्रशिक्षित किया गया। सीओ और कुल सिनगैस खपत दर की एक समान भविष्यवाणी प्रवृत्ति एक जटिल गैस-ठोस प्रतिक्रिया के कैनेटीक्स के मॉडलिंग में मशीन सीखने की प्रयोज्यता के लिए सबूत प्रदान करती है।

CONTENTS

1 INTRODUCTION	1
1.1 RESEARCH BACKGROUND	3
1.1.1 <i>Energy Consumption: World View</i>	3
1.1.2 <i>Fuel for the transportation sector</i>	4
1.2 DIESEL PRODUCTION	5
1.3 DIESEL PRODUCTION FROM RENEWABLE RESOURCES	6
1.3.1 <i>Fatty Acid Methyl Ester or biodiesel</i>	6
1.3.2 <i>Green diesel</i>	7
1.3.3 <i>White diesel</i>	8
1.3.4 <i>Fischer-Tropsch diesel</i>	8
1.4 RESEARCH MOTIVATION	10
1.5 RESEARCH OBJECTIVES	12
1.6 THESIS OVERVIEW	12
2 LITERATURE REVIEW	15
2.1 A HISTORICAL OVERVIEW	17
2.2 FISCHER-TROPSCH PROCESS	18
2.2.1 <i>Composition of syngas</i>	19
2.2.2 <i>Fischer-Tropsch reaction networks</i>	21
2.2.3 <i>Influence of Process parameters upon FT activity and selectivity</i>	22
2.2.4 <i>Product distribution in FT synthesis</i>	24
2.2.5 <i>Possibilities of using low Ribblet ratio syngas in FT reaction</i>	26
2.2.6 <i>Liquid Product Upgradation</i>	27
2.3 CATALYSTS FOR FISCHER-TROPSCH SYNTHESIS	29
2.3.1 <i>Bimetallic catalyst composition and FT performance</i>	30
2.3.2 <i>Structural Activity Relationship</i>	33
2.3.3 <i>Deactivation behaviour of Fe-Co bimetallic catalyst</i>	34
2.3.4 <i>Catalyst for low Ribblet ratio syngas</i>	35
2.4 EFFECT OF CATALYST SUPPORT	38
2.4.1 <i>Metal oxides</i>	39
2.4.2 <i>Mesoporous supports</i>	40
2.4.3 <i>Carbon supports</i>	40
2.4.4 <i>Zeolites based support</i>	42
2.5 REACTION MECHANICS AND KINETICS	44

2.5.1 Fischer-Tropsch mechanism.....	44
2.5.2 Fischer-Tropsch kinetics.....	47
2.6 LITERATURE LACUNAE	53
2.7 SPECIFIC RESEARCH OBJECTIVES	53
3 EXPERIMENTAL.....	55
3.1 INTRODUCTION.....	57
3.2 CATALYST SYNTHESIS	57
3.2.1 Synthesis of catalyst supports	57
3.2.2 Synthesis of Fe-Co bimetallic nanoparticles	61
3.3 CATALYST CHARACTERISATION	62
3.3.1 Crystallographic Techniques.....	63
3.3.2 Spectroscopic Techniques.....	64
3.3.3 Microscopic Techniques	65
3.3.4 Physico-chemical analysis	66
3.3.5 Solid-state Nuclear Magnetic Resonance	67
3.3.6 Thermal analysis.....	67
3.3.7 Diffuse Reflectance Infrared Spectroscopy.....	68
3.4 FIXED-BED REACTOR SET-UP	69
3.4.1 Catalyst activity testing.....	71
3.4.2 Evaluation of mass transfer limitations	72
3.4.3 Evaluation of heat transfer limitations	73
3.5 LIQUID PRODUCT CHARACTERISATION	74
3.5.1 Simulated Distillation	74
3.5.2 Gas Chromatography-Mass Spectrometer (GC-MS).....	75
3.5.3 FT-IR analysis.....	75
3.5.4 Elemental analysis	75
3.6 SPENT CATALYST CHARACTERISATION	76
4 RESULTS AND DISCUSSION.....	77
4.1 SYNERGISTIC EFFECT OF HIERARCHICAL HZSM-5 SUPPORTED FE-CO CATALYST..	79
4.1.1 Introduction.....	79
4.1.2 Characterisations of parent HZSM-5 and desilicated HZSM-5	80
4.1.3 Effect of Fe-Co ratio	86
4.1.4 Effect of mesoporosity in the catalyst support	92
4.1.5 Effect of reaction temperature	93

4.1.6 Catalytic activity comparison	94
4.2 CO ₂ FORMATION IN FISCHER–TROPSCH SYNTHESIS	96
4.2.1 Introduction.....	96
4.2.2 Mechanistic studies.....	96
4.2.3 CO binding mechanism.....	98
4.2.4 WGS activity on Fe ₃ O ₄ (111) and Co ₃ O ₄ (111) surface.....	99
4.2.5 Boudouard activity on χ -Fe ₅ C ₂ (111) and Co ₂ C (111) surface	100
4.2.6 Effect of Fe-Co bimetallic phases in the reaction mechanisms	100
4.2.7 Acidity comparison of active sites.....	102
4.3 IMPACT OF MEDIUM PORE SILICA-ALUMINA SUPPORTS ON FT PERFORMANCE	106
4.3.1 Introduction.....	106
4.3.2 Phase elucidation by wide-angle X-ray diffraction and X-ray photoelectron spectroscopy.....	107
4.3.3 ²⁷ Al and ²⁹ Si solid-state Nuclear Magnetic Resonance	109
4.3.4 TEM for morphological analysis at the nanoscale	110
4.3.5 NH ₃ -Temperature Programmed Desorption.....	111
4.3.6 Influence of pore diameter, crystallite size upon FT activity.....	112
4.3.7 Correlation of product selectivity with support surface acidity	113
4.4 RATIONAL DESIGN OF PROCESS PARAMETERS.....	114
4.4.1 Introduction.....	114
4.4.2 Experimental design and statistical optimization	115
4.4.3 The regression model.....	116
4.4.4 Response Surface methodology and Regression analysis.....	116
4.4.5 Second-order equation fitting	117
4.4.6 Analysis of Variance of response (ANOVA analysis)	118
4.4.7 Percentage Contribution of variables by ANOVA analysis.....	118
4.4.8 Diagnostics plots for the regression model.....	119
4.4.9 Three-dimensional surface and counterplots.....	120
4.4.10 Desirability and experimental validation of the empirical models.....	123
4.4.11 Liquid product characterization	124
4.4.12 Spent catalyst characterizations	126
4.5 INVESTIGATIONS ON OLEFIN TO PARAFFIN RATIO IN C ₂ -C ₃ RANGE OF HYDROCARBONS	128
4.5.1 Introduction.....	128

4.5.2 Olefin (O_n)/ paraffin (P_n) ratios of light hydrocarbons for different carbon monoxide conversion	128
4.5.3 The relation between olefin $_{n+1}$ /olefin $_n$ and paraffin $_{n+1}$ /paraffin $_n$ with CO conversion.....	130
4.6 MOLECULAR-SCALE INVESTIGATIONS ON THE SPATIAL ARRANGEMENT OF FUNCTIONALITIES.....	132
4.6.1 Introduction.....	132
4.6.2 Crystal analysis and structural characterization	133
4.6.3 Influence of Fe-Co proximity upon Reduction behavior.....	136
4.6.4 Morphological, Textural and Elemental features	139
4.6.5 FT activity of different Fe and Co proximity	141
4.6.6 Rationally controlled WGS activity through Fe-Co proximity	142
4.6.7 Impact of Fe-Co spatial separation on hydrocarbon distribution.....	143
4.6.8 Increasing proximity between FeCo ₂ O ₄ and support.....	144
4.6.9 Stability testing of different Fe-Co catalyst-bed configurations.....	145
4.6.10 Spent catalyst characterization.....	146
CONCLUSION.....	149
5 REACTION MECHANISM AND KINETIC STUDY	151
5.1 INTRODUCTION.....	153
5.2 TRANSIENT DRIFTS-MS OPERANDO STUDIES.....	154
5.2.1 CO adsorption over supported Fe-Co surface.....	154
5.2.2 In-situ studies of FT reaction over supported Fe-Co surface.....	155
5.3 MECHANISTIC INSIGHTS OF FISCHER-TROPSCH REACTION KINETICS	158
5.4 DISCRIMINATION OF LITERATURE REPORTED KINETIC MODELS	161
5.5 MECHANISTIC INSIGHTS OF COMBINED FISCHER-TROPSCH AND WATER-GAS SHIFT REACTION KINETICS	163
CONCLUSION.....	167
6 IMPLEMENTING MACHINE LEARNING IN KINETIC DATA INTERPRETATION	169
6.1 INTRODUCTION.....	171
6.2 METHODOLOGY	172
6.3 PEARSON CORRELATION ANALYSIS	173
6.3.1 Linear regression.....	175
6.4 BACK PROPAGATION NEURAL NETWORK	176

6.5 REACTION KINETICS.....	178
6.6 PREDICTIVE CAPABILITY OF BP NEURAL NETWORK.....	179
CONCLUSION.....	179
7 CONCLUSIONS AND FUTURE WORK RECOMMENDATIONS.....	181
7.1 THESIS CONCLUSION.....	183
7.2 FUTURE WORK RECOMMENDATIONS.....	186
8 REFERENCES.....	189
9 APPENDICES.....	223
10 ABOUT THE AUTHOR.....	247

LIST OF TABLES

TABLE 1 CHARACTERISTICS OF DIESEL PRODUCED FROM DIFFERENT RENEWABLE RESOURCES [12].	10
TABLE 2 SUMMARY OF BIMETALLIC CATALYST EMPLOYED IN FISCHER-TROPSCH SYNTHESIS.	32
TABLE 3 SUMMARY OF CATALYST EMPLOYED IN FISCHER-TROPSCH SYNTHESIS USING LOW RIBBLET RATIO SYNGAS.	37
TABLE 4 LITERATURE RATE EXPRESSIONS AND ACTIVATION ENERGY IN FT REACTION OVER BIMETALLIC/ TRIMETALLIC CATALYSTS.	49
TABLE 5 SURFACE ACIDITY MEASUREMENTS USING NH ₃ -TPD AND PYRIDINE- IR STUDIES.	86
TABLE 6 FT PERFORMANCE OF DIFFERENT FE/CO RATIO ACTIVE METAL SUPPORTED OVER HIERARCHICAL HZSM-5.	90
TABLE 7 COMPARISON OF CATALYTIC PERFORMANCES OF SYNTHESISED BIMETALLIC CATALYSTS WITH LITERATURE REPORTED CATALYSTS FOR FT REACTION USING LOW RIBBLET RATIO SYNGAS.	94
TABLE 8 STRUCTURAL PARAMETERS AND BINDING ENERGY OF CO ADSORPTION MECHANISM OVER DIFFERENT METALLIC SURFACES.	99
TABLE 9 ADSORPTION ENERGY (E_{ADS}), ELECTROSTATIC SURFACE POTENTIAL MAXIMA ($V_{\text{s,MAX}}$) AND ELECTROPHILIC FUKUI FUNCTION (F^+) OVER DIFFERENT METALLIC SURFACES.	102
TABLE 10 CO AND CO ₂ CONVERSION OVER DIFFERENT CATALYSTS.	105
TABLE 11 BINDING ENERGY (eV) OF FE 2P _{3/2} , FE2P _{1/2} , CO 2P _{3/2} AND CO 2P _{1/2} ALONG WITH THE ATOMIC RATIO OF FE/CO DETERMINED BY XPS ANALYSIS.	108
TABLE 12 PHYSICOCHEMICAL PROPERTIES OF SUPPORTS AND FE-CO METAL LOADED CATALYSTS.	109
TABLE 13 SURFACE ACIDITY MEASUREMENTS USING NH ₃ -TPD.	112
TABLE 14. LIST OF EXPERIMENTAL FACTORS WITH THE SYMBOLS AND CODED LEVELS FOR THE RANGES ADOPTED FOR THE STUDY.	115

TABLE 15 CHARACTERIZATION OF DEPOSITED CARBONACEOUS MATERIAL OVER 120 HOURS OF TIME-ON-STREAM SPENT CATALYST.	127
TABLE 16 BINDING ENERGY DETERMINED BY X-RAY PHOTOELECTRON STUDY OF AS-CALCINED AND IN-SITU REDUCED CATALYSTS.....	138
TABLE 17 TEXTURAL PROPERTIES AND ELEMENTAL COMPOSITION OF LABORATORY AS-CALCINED CATALYSTS.	140
TABLE 18 FT PERFORMANCE OF SUPPORTED FE AND CO PARTICLES ARRANGED IN DIFFERENT PROXIMITY CATALYST-BED CONFIGURATIONS.....	142
TABLE 19 REACTION RATES OF FT AND WGS REACTION OBTAINED IN THE DIFFERENT CATALYST-BED CONFIGURATIONS.....	143
TABLE 20 AVERAGE PARTICLE SIZE AND METAL DISPERSION OF FRESH AND 120 HOURS CATALYTIC RUN SPENT CATALYST.	149
TABLE 21 ELEMENTARY REACTIONS AND THE RATE EXPRESSIONS WITH MAPD VALUES BASED ON THE DIFFERENT REACTION MECHANISMS.	159
TABLE 22 KINETIC AND THERMODYNAMIC PARAMETERS CALCULATED FROM FT-III3, FT-III4 AND FT-IV5 RATE EXPRESSIONS.	161
TABLE 23 MAPD VALUES FOR LITERATURE REPORTED IRON AND COBALT CATALYST. .	162
TABLE 24 STATISTICAL SIGNIFICANCE, KINETIC AND THERMODYNAMIC PARAMETERS CALCULATED FROM COMBINED FT AND WGS RATE EXPRESSIONS.	166
TABLE 25 PEARSON CORRELATION ANALYSIS ON H ₂ /CO/CO ₂ CONVERSIONS.....	175
TABLE 26 COMBINATIONS OF INPUT NODES FOR BP NEURAL NETWORKS.....	175
TABLE 27 COEFFICIENTS OF 5 PARAMETERS AND 4 PARAMETERS LINEAR REGRESSION ANALYSIS.....	175
TABLE 28 RATE EXPRESSION USED IN THE PRESENT STUDY.....	178

LIST OF FIGURES

FIGURE 1 HISTORY AND PREDICTED ENERGY CONSUMPTION BY NON-ORGANISATION OF ECONOMIC CO-OPERATION AND DEVELOPMENT (OECD) REGIONS (ADAPTED FROM [2]).....	3
FIGURE 2 FOSSIL FUELS RESERVE TO PRODUCTION RATIO. (ADAPTED FROM [3]).	4
FIGURE 3 GLOBAL CONSUMPTION OF TRANSPORTATION FUEL AND CONSUMPTION OF DIESEL FUEL BY END-USE. (ADAPTED FROM [9]).	5
FIGURE 4 DISTRIBUTION OF PRODUCTS GENERATED FROM DISTILLATION OF ONE BARREL OF CRUDE OIL.	5
FIGURE 5 TRANSESTERIFICATION OF VEGETABLE OIL FOR BIODIESEL PRODUCTION.	7
FIGURE 6 HYDROPROCESSING OF VEGETABLE OILS AND FATS FOR GREEN DIESEL SYNTHESIS.	7
FIGURE 7 SCHEMATICS OF XTL PROCESS (X=BIOMASS, COAL AND NATURAL GAS).	9
FIGURE 8 PROPOSED SCHEMATICS OF FISCHER-TROPSCH PROCESS WITH LOW RIBBLET RATIO SYNGAS FEEDSTOCK.	11
FIGURE 9 GENERIC REPRESENTATION OF A TYPICAL FISCHER-TROPSCH PROCESS.....	19
FIGURE 10 SYNGAS COMPOSITION FROM DIFFERENT FEEDSTOCKS [39].....	20
FIGURE 11 (A) CARBON NUMBER DISTRIBUTION BASED ON THE IDEAL ASF DISTRIBUTION AND (B) DEVIATIONS FROM CLASSICAL ASF DISTRIBUTION MODEL [58].	24
FIGURE 12 MONOMOLECULAR AND BIMOLECULAR MECHANISMS FOR HYDROCRACKING SATURATED HYDROCARBONS. REPRODUCED FROM REFERENCE [75].	28
FIGURE 13 SCHEMATIC OF THE REACTIONS OCCURRING OVER FT ACTIVE SITES (BLACK COLOUR) AND THE ACTIVE ZEOLITE SITES (BLUE COLOUR). ADAPTED FROM [148]. .	42
FIGURE 14 SCHEMATIC OF THE ALKYL MECHANISM.	45
FIGURE 15 SCHEMATIC OF ALKENYL MECHANISM.	46
FIGURE 16 SCHEMATIC OF CO INSERTION MECHANISM.....	47
FIGURE 17 SCHEMATICS OF HZSM-5 SYNTHESIS PROCEDURE.	58
FIGURE 18 SCHEMATICS OF HIERARCHICAL HZSM-5 SYNTHESIS PROCEDURE.	58
FIGURE 19 SCHEMATICS OF MESOPOROUS SILICA SYNTHESIS PROCEDURE.	59

FIGURE 20 SCHEMATICS OF MESOPOROUS ALUMINA PROCEDURE.	60
FIGURE 21 SCHEMATICS OF ALUMINA DOPED MESOPOROUS SILICA PROCEDURE.	61
FIGURE 22 UNIT CELL STRUCTURE OF FeCO_2O_4 GENERATED BY WIDE-ANGLE XRD REFINEMENT DATA.	62
FIGURE 23 PROCESS FLOW SCHEME OF THE EXPERIMENTAL SET-UP USED FOR FISCHER- TROPSCH SYNTHESIS. (MFC: MASS FLOW CONTROLLER; SRV: SAFETY RELIEF VALVE; PMH: PRE-MIXER HEATER; PI: PRESSURE INDICATOR; TC: TEMPERATURE CONTROLLER; TI: TEMPERATURE INDICATOR; BPR: BACK PRESSURE REGULATOR; GC: GAS CHROMATOGRAPHY).	70
FIGURE 24(A) XRD PATTERNS AND SOLID-STATE NMR SPECTRA (B) ^{27}Al AND (C) ^{29}Si OBTAINED FROM PARENT HZSM-5 AND ORGANIC BASE TREATED <i>HIERARHZSM-5</i>	80
FIGURE 25 SEM IMAGES OF CALCINED PARENT (A) HZSM-5 AND (B) <i>HIERARHZSM-5</i>	82
FIGURE 26 HR-TEM IMAGES OF CALCINED (A) PARENT HZSM-5, (B) <i>HIERARHZSM-5</i> , FFT PATTERNS CORRESPONDING TO THE SELECTED REGION OF (C) PARENT HZSM-5 AND (B) <i>HIERARHZSM-5</i>	82
FIGURE 27(A) FT-IR SPECTRA OF CALCINED PARENT HZSM-5 AND DESILICATED <i>HIERARHZSM-5</i> AND (B) OH GROUPS FOR THE PARENT AND DESILICATED HZSM-5 ZEOLITES AT 200°C.....	83
FIGURE 28 IN-SITU DRIFTS SPECTRA OF PARENT HZSM-5 AND <i>HIERARHZSM-5</i> AFTER DEGASSING OF PYRIDINE AT (A) 200 °C AND (B) 350 °C.	85
FIGURE 29 NH_3 -TPD PROFILES OF (A) PARENT HZSM-5 AND (B) <i>HIERARHZSM-5</i>	85
FIGURE 30 (A) X-RAY DIFFRACTION PATTERN (B) N_2 ADSORPTION-DESORPTION ISOTHERMS OF SYNTHESIZED CATALYSTS. (I) $\text{Fe}/\textit{HIERARHZSM-5}$, (II) $2\text{Fe-Co}/\textit{HIERARHZSM-5}$; (III) $\text{Fe Co}/\textit{HIERARHZSM-5}$, (IV) $\text{Fe-2Co}/\textit{HIERARHZSM-5}$, (V) $\text{Co}/\textit{HIERARHZSM-5}$, (VI) $\text{Fe-2Co}/\text{HZSM-5}$	87
FIGURE 31 H_2 -TPR OF (A) $\text{Fe}/\textit{HIERARHZSM-5}$, (B) $2\text{Fe-Co}/\textit{HIERARHZSM-5}$; (C) Fe- $\text{Co}/\textit{HIERARHZSM-5}$, (D) $\text{Fe-2Co}/\textit{HIERARHZSM-5}$, (E) $\text{Co}/\textit{HIERARHZSM-5}$	88
FIGURE 32 (A) HYDROCARBON PRODUCT SELECTIVITY FOR THE FT REACTION PERFORMED ON THE LABORATORY SYNTHESISED Fe-Co BIMETALLIC CATALYSTS SUPPORTED OVER <i>HIERARHZSM-5</i> AND CONVENTIONAL HZSM-5, (B) QUANTITATIVE DISTRIBUTION OF CONDENSED LIQUID PRODUCTS USING ASTM D2887.	90

FIGURE 33 (A) THERMOGRAVIMETRIC ANALYSIS OF SPENT CATALYST AFTER 72 HOURS OF TIME-ON-STREAM (B) TIME-OF-STREAM CO CONVERSION.	93
FIGURE 34 EFFECT OF TEMPERATURE ON % CO CONVERSION, METHANE (C ₁) AND C ₅₊ YIELD AT 20 BAR, WITH LOW RIBBLET RATIO SYNGAS ON FE-2CO/HIERARHZSM-5.....	93
FIGURE 35 DENSITY OF STATES (DOS) PROFILE OF FREE CO AND ADSORBED CO ON DIFFERENT METAL SURFACES.	98
FIGURE 36 GEOMETRY OPTIMIZED STRUCTURES OF THE REACTANTS AND PRODUCTS ON DIFFERENT METAL SURFACES: CO AND H ₂ O OVER FE ₃ O ₄ (111) (A) SIDE-VIEW (B) TOP-VIEW; CO ₂ AND H ₂ ON FE ₃ O ₄ (111) (C) SIDE-VIEW (D) TOP-VIEW; CO AND H ₂ O OVER CO ₃ O ₄ (111) (E) SIDE-VIEW (F) TOP-VIEW; CO ₂ AND H ₂ OVER CO ₃ O ₄ (111) (G) SIDE-VIEW (H) TOP-VIEW	99
FIGURE 37 GEOMETRY OPTIMIZED STRUCTURES OF THE REACTANTS AND PRODUCTS ON DIFFERENT METAL SURFACES: CO ON X-FE ₅ C ₂ (111) (A) SIDE-VIEW (B) TOP-VIEW; CO ₂ AND C ON X-FE ₅ C ₂ (111) (C) SIDE-VIEW (D) TOP-VIEW; CO OVER CO ₂ C (111) (E) SIDE-VIEW (F) TOP-VIEW; CO ₂ AND C ON CO ₂ C (111) (G) SIDE-VIEW (H) TOP-VIEW.....	100
FIGURE 38 GEOMETRY OPTIMIZED STRUCTURES OF THE REACTANTS AND PRODUCTS ON DIFFERENT METAL SURFACES: CO AND H ₂ O ON FE-CO (111) (A) SIDE-VIEW (B) TOP-VIEW; CO ₂ AND H ₂ OVER FE-CO (111) (C) SIDE-VIEW (D) TOP-VIEW; CO AND H ₂ O OVER FE-CO (110) (E) SIDE-VIEW (F) TOP-VIEW; CO ₂ AND H ₂ OVER FE-CO (110) (G) SIDE-VIEW (H) TOP-VIEW. GEOMETRY OPTIMIZED STRUCTURES OF THE REACTANTS AND PRODUCTS ON DIFFERENT METAL SURFACES: CO ON FE-CO (111) (I) SIDE-VIEW (J) TOP-VIEW; CO ₂ AND C ON FE-CO (111) (K) SIDE-VIEW (L) TOP-VIEW; CO ON FE-CO (110) (M) SIDE-VIEW (N) TOP-VIEW; CO ₂ AND C ON FE-CO (110) (O) SIDE-VIEW (P) TOP-VIEW.	101
FIGURE 39 PYRIDINE ADSORPTION IN-SITU DRIFTS SPECTRA OF DIFFERENT CATALYSTS.	105
FIGURE 40 (A) LOW-ANGLE X-RAY SCATTERING (B) WIDE-ANGLE X-RAY DIFFRACTION.	107
FIGURE 41(A) ²⁷ AL AND (B) ²⁹ SI SOLID-STATE NMR OF DIFFERENT SILICA-ALUMINA SUPPORT SAMPLES.....	110
FIGURE 42 TEM IMAGES OF THE DIFFERENT SILICA-ALUMINA SUPPORT (A) MS, (B) AMS, (C) MA, (D) ZTM AND (E) ZPM.....	111

FIGURE 43 CO CONSUMPTION RATE AS A FUNCTION OF THE RATIO OF FE-CO CRYSTALLITE SIZE AND SUPPORT PORE VOLUME.	113
FIGURE 44 (A) CH ₄ SELECTIVITY AS A FUNCTION OF VERY STRONG ACIDIC SITES OF THE CATALYST SUPPORT (B) C ₈ -C ₂₀ WEIGHT % AS A FUNCTION OF INTERMEDIATE ACIDIC SITES OF THE CATALYST SUPPORT.	114
FIGURE 45 PERCENTAGE CONTRIBUTION OF LINEAR, SQUARE AND SECOND-ORDER INTERACTION TERMS UPON (A) CO CONSUMPTION RATE, (B) CH ₄ SELECTIVITY AND (C) C ₅₊ HYDROCARBONS SELECTIVITY.	118
FIGURE 46 3-DIMENSIONAL SURFACE AND CONTOUR PLOTS FOR MAXIMISING CO CONSUMPTION RATE (A) EFFECT OF RT AND RP, (B) RT AND RR, (C) RP AND SV, (D) RT AND SV, (E) RP AND RR, (F) SV AND RR.	120
FIGURE 47 3-DIMENSIONAL SURFACE AND CONTOUR PLOTS FOR MINIMISING CH ₄ SELECTIVITY (A) EFFECT OF RT AND RP, (B) RT AND RR, (C) RP AND SV, (D) RT AND SV, (E) RP AND RR, (F) SV AND RR.	122
FIGURE 48 3-DIMENSIONAL SURFACE AND CONTOUR PLOTS FOR MAXIMISING C ₅₊ SELECTIVITY (A) EFFECT OF RT AND RP, (B) RT AND RR, (C) RP AND SV, (D) RT AND SV, (E) RP AND RR, (F) SV AND RR.	123
FIGURE 49 OPTIMISATION RESULTS OF ENHANCED FT ACTIVITY AND SELECTIVITY UNDER LOW RIBBLET RATION SYNGAS.	124
FIGURE 50 (A) SIMULATED DISTILLATION CURVES OF DIESEL OBTAINED FROM FT SYNTHESIS AT OPTIMAL PROCESS CONDITIONS AND THE CONVENTIONAL CRUDE BASED DIESEL. (B) THE CARBON NUMBER DISTRIBUTION IN THE LIQUID HYDROCARBONS OBTAINED AS AN FT PRODUCT AT OPTIMAL PROCESS CONDITIONS. (REACTION TEMPERATURE= 240°C, REACTOR PRESSURE= 23 BAR (G), SPACE-VELOCITY= 2592 mL H ⁻¹ G _{CAT} ⁻¹ AND RIBBLET RATIO= 0.5).	125
FIGURE 51 ATR-FTIR SPECTRUM OF LIQUID FUEL FORMED AT OPTIMAL FISCHER-TROPSCH PROCESS PARAMETERS (B) THERMOGRAVIMETRIC ANALYSIS (TGA) AND DIFFERENTIAL THERMAL ANALYSIS (DTA) OF 120 HOURS OF TIME-ON-STREAM SPENT CATALYST AT OPTIMAL PROCESS PARAMETERS.	126
FIGURE 52 OLEFIN TO PARAFFIN RATIO FOR THE C ₂ -C ₅ RANGE OF HYDROCARBONS FOR DIFFERENT CARBON MONOXIDE CONVERSIONS. (TEMPERATURE ARE INDICATED BY FILLING OF THE SYMBOL (220°C - FILLED SYMBOLS; 240°C - OPEN SYMBOLS; 260°C -	

CROSSED OPEN SYMBOLS); COLOURS REPRESENT THE CHAIN LENGTH (C ₂ — BLACK, C ₃ — RED, C ₄ — BLUE, C ₅ - GREEN).	129
FIGURE 53 RELATION BETWEEN O_{N+1}/O_N AND P_{N+1}/P_N WHEN $N=2$ WITH CO CONVERSION.	130
FIGURE 54 VARIATION OF THE RELATIVE MOLAR COMPOSITION OF C ₃ /C ₂ (OLEFIN+ PARAFFIN) WITH CO CONVERSION.	131
FIGURE 55 WIDE-ANGLE X-RAY DIFFRACTION PATTERN OF (A) AS-CALCINED <i>HIERARHZSM-5</i> SUPPORT, (B) IRON AND COBALT ARRANGED IN A DIFFERENT PROXIMITY.	133
FIGURE 56 STRUCTURAL CHARACTERISATION OF LABORATORY SYNTHESISED NANO-SIZED FeCo ₂ O ₄ (A) RIETVELD REFINEMENT OF WIDE-ANGLE XRD (B) UNIT CELL STRUCTURE OF FeCo ₂ O ₄ GENERATED BY WIDE-ANGLE XRD REFINEMENT DATA (C) RAMAN SPECTRUM (D) UV-VISIBLE DIFFUSE REFLECTANCE SPECTRUM (E) XPS SPECTRUM IN THE RANGE OF Fe2p, Co2p AND O1s (F) FE-SEM IMAGE WITH EDX RESULTS.....	136
FIGURE 57 HYDROGEN-TEMPERATURE PROGRAM REDUCTION PROFILES OF AS-CALCINED (A) Fe/ <i>HIERARHZSM-5</i> , (B) Co/ <i>HIERARHZSM-5</i> , (C) Fe+Co/ <i>HIERARHZSM-5</i> (<i>PHYSICAL MIX</i>) AND (D) FeCo ₂ O ₄ / <i>HIERARHZSM-5</i> (<i>CHEMICAL MIX</i>).	137
FIGURE 58 HIGH-RESOLUTION TRANSMISSION ELECTRON MICROSCOPY IMAGES OF THE AS-CALCINED CATALYSTS WITH CORRESPONDING SELECTED AREA ELECTRON DIFFRACTION (SAED) PATTERN (INSIGHT). (A) Fe/ <i>HIERARHZSM-5</i> , (B) Co/ <i>HIERARHZSM-5</i> , (C) Fe+Co <i>HIERARHZSM-5</i> (<i>PHYSICAL MIX</i>) (D) FeCo ₂ O ₄ / <i>HIERARHZSM-5</i> (<i>CHEMICAL MIX</i>), (E) UNSUPPORTED FeCo ₂ O ₄ , (F) <i>HIERARHZSM-5</i>	139
FIGURE 59 DIFFERENT PACKED-BED CONFIGURATIONS USED IN THE PRESENT WORK.....	141
FIGURE 60 (A) SIMULATED DISTILLATION CHARACTERISTICS OF THE COLLECTED CARBON-NEUTRAL SYNTHETIC FUEL, (B) SELECTIVITY OF GASOLINE, JET FUEL, DIESEL AND LUBRICATING OIL IN LIQUID FUEL COLLECTED AFTER 120 HOURS' TIME-OF-STREAM IN DIFFERENT CATALYST-BED CONFIGURATIONS. *ASF PREDICTED PRODUCT SELECTIVITY WITH CHAIN-GROWTH PROBABILITY (A= 0.9) [278].	144
FIGURE 61 (A) 120 HOURS OF TIME-ON-STREAM CATALYST-TIME-YIELD STABILITY (B) CARBON CONTENT AND CARBON FORMATION RATE DIFFERENT CONFIGURATIONS OF	

CATALYST-BEDS DESIGN AT REACTION TEMPERATURE: 240°C; REACTOR PRESSURE: 23 BAR; SPACE VELOCITY: 2592 mLH ⁻¹ G _{CAT} ⁻¹	145
FIGURE 62 X-RAY DIFFRACTOGRAM AFTER 120 HOURS OF THE FT REACTION (A) PHYSICALLY MIXED FE+CO AND (B) FeCO ₂ O ₄ /HIERARHZSM-5.	147
FIGURE 63 THERMOGRAVIMETRIC ANALYSIS OF THE SPENT CATALYST OF 120 HOURS OF TIME-ON-STREAM.....	147
FIGURE 64 TEM AND EDX ANALYSIS OF (A) FRESH AND (B) SPENT CATALYST.	148
FIGURE 65 (A) DRIFTS SPECTRA OF CO ADSORPTION WITH TIME OVER FE-CO; (B) DECONVOLUTED AND SECOND DERIVATIVE IR SPECTRUM IN THE RANGE OF 2300-1700 CM ⁻¹	154
FIGURE 66 DRIFTS SPECTRA RECORDED DURING THE REACTION (A) 3100-2700 CM ⁻¹ SHOWING DIFFERENT N-(C-H) STRETCHING VIBRATIONS AND (B) 1750-1350 CM ⁻¹ DEPICTING PEAKS ASSOCIATED WITH THE N-(C-O) STRETCHING AND Δ-(C-H) BENDING VIBRATIONS OF HCO/HCOO ⁻ INTERMEDIATE SPECIES.....	156
FIGURE 67 (A) DECONVOLUTED AND SECOND DERIVATIVE IR SPECTRUM 3100-2700 CM ⁻¹ ; (B) AND (C) EVOLUTION OF PEAK AREA AND HEIGHT ASCRIBING TO N-(C-H) AND Δ-(C-H) MODES.	156
FIGURE 68 POSSIBLE PATHWAYS OF CO DISSOCIATION AND CH ₄ FORMATION OVER SUPPORTED FE-CO CATALYST SURFACE BASED ON THE OPERANDO STUDIES.	158
FIGURE 69 PARITY PLOTS FOR COMPARING EXPERIMENTAL VERSUS CALCULATED RATE BASED ON (A) FT-III3, (B) FT-III4, AND (C) FT-IV5 RATE EXPRESSIONS.	160
FIGURE 70 REACTION SCHEMES IN THE PROPOSED COMPREHENSIVE FT-III4/WGS-I MODEL.	164
FIGURE 71 PARITY PLOTS COMPARE EXPERIMENTAL VERSUS MODELLED (A) CO CONSUMPTION IN FT AND WGS AND (B) SYNGAS CONSUMPTION RATE BASED ON FT-III4/WGS-I RATE EXPRESSIONS.	165
FIGURE 72 BP NEURAL NETWORK MODEL FOR PREDICTING THE CO, H ₂ AND CO ₂ CONVERSION.	173
FIGURE 73 FORWARD AND BACKWARD PROPAGATION IN BP NEURAL NETWORK FOR ERROR MINIMISATION.....	173

FIGURE 74 HEAT-MAP OF THE PEARSON CORRELATION ANALYSIS ON CO, H ₂ AND TOTAL SYNGAS CONSUMPTION RATE.	174
FIGURE 75 PARITY PLOTS BETWEEN EXPERIMENTAL AND TRAINED AND TESTED FIVE PARAMETERS, FOUR-PARAMETER AND BP NEURAL NETWORK REGRESSION ANALYSIS, PREDICTED VALUES.	176
FIGURE 76 THE COMPARISON OF ROOT MEAN SQUARE ERROR (RMSE) OF TRAINED AND TESTED DATA AND FIVE-PARAMETER LINEAR REGRESSION, FOUR-PARAMETER LINEAR REGRESSION AND BP NEURAL NETWORK DATA.	177
FIGURE 77 PARITY PLOTS TO COMPARE THE PREDICTABILITY OF OPTIMISED BP NEURAL NETWORK.	178
FIGURE 78 COMPARISON OF THE BP NEURAL NETWORK DATA PREDICTIONS WITH LHHW KINETIC MODEL FT-III4/WGS-I.	179

PERMISSION

The permission from the respective journals has been taken for the publications which are included in this thesis.

List of publications related to the thesis till the date of submission.

PEER-REVIEWED JOURNAL PUBLICATIONS

1. **Shashank Bahri**, Uttaran Basak, Sreedevi Upadhyayula; Rational design of process parameters for carbon-neutral and sulfur-free motor fuel production from second-generation biomass generated syngas; *Journal of Cleaner Production*, 279 (2021), 123559 <https://doi.org/10.1016/j.jclepro.2020.123559> (Impact Factor 9.3)
2. **Shashank Bahri**, Sreedevi Upadhyayula; Experimental investigations on olefin to paraffin ratio in Fischer-Tropsch products using syngas of low Ribblet ratio; *Catalysis Today*, 348 (2020), 55-62. <https://doi.org/10.1016/j.cattod.2019.08.039>. (Impact Factor 6.8)
3. **Shashank Bahri**, Anna Maria Venezia, Sreedevi Upadhyayula; Utilization of greenhouse gas carbon dioxide for cleaner Fischer-Tropsch diesel production; *Journal of Cleaner Production*, 228 (2019), 1013-1024 <https://doi.org/10.1016/j.jclepro.2019.04.310>. (Impact Factor 9.3)
4. **Shashank Bahri**, Tanmoy Patra, Sonal, Sreedevi Upadhyayula; Synergistic effect of bifunctional mesoporous ZSM-5 supported Fe-Co catalyst for selective conversion of syngas with low Ribblet ratio into synthetic fuel; *Microporous and Mesoporous Materials*, 275 (2019), 1-13. <https://doi.org/10.1016/j.micromeso.2018.08.004>. (Impact Factor 5.5)

LIST OF APPENDICES

APPENDIX-I.....	225
APPENDIX-II	231
APPENDIX-III	243